Optimal Fuel Consumption in Solid Oxide Fuel Cell based Hybrid Electric Tractor Using Improved Walrus Optimization Technique (IWaOT)

Ajay Ahuja[1], Dr. D. R. Waghole[2], Dr. Sushil S. Ramdasi[3]

[1]*Research Scholar, Dr. Vishwanath Karad MIT World Peace University, Pune, Maharashtra India.*
[2]*Associate Professor, Dr. Vishwanath Karad MIT World Peace University, Pune, Maharashtra India.*
[3]*Deputy Director, Automotive Research Association of India, Pune, Maharashtra, India.*
Email: ajay_design@hotmail.com

Abstract: The global demand for electrical energy is rising rapidly due to industrialization and modernization. While fossil fuels are commonly used to meet this demand, their drawbacks—such as global warming, limited availability, and harmful emissions—restrict their long-term use. To address these challenges, there is a growing need for sustainable and environmentally friendly energy sources. Over the past two decades, fuel cells have gained significant attention as a renewable energy option due to their zero-emission operation and high efficiency. Among them, the solid oxide fuel cell (SOFC) stands out for its high operating efficiency and temperature. SOFCs are particularly advantageous because they can directly utilize natural gas. Known for their versatility and quick response, SOFCs are increasingly seen by manufacturers as a promising solution for generating electrical energy.

This research proposes an improved approach to enhance efficiency and reduce fuel consumption in Solid Oxide Fuel Cell-based Hybrid Electric Tractors (SOFC-HET). Central to this strategy is the use of the Improved Walrus Optimization Technique (IWaOT), a predictive controller designed to anticipate the tractor's power demand and the fuel cell's operating conditions. By leveraging these predictions, IWaOT optimizes key control parameters, including power distribution, fuel flow, air flow, and temperature. This targeted optimization not only reduces hydrogen fuel consumption but also improves overall efficiency and extends the fuel cell system's lifespan.

Keywords: Fuel consumption, Solid Oxide Fuel Cell, Hybrid Electric Tractors, Battery capacity, Hydrogen consumption, and Electricity usage

1. Introduction

The electrification of agricultural machinery encompasses research on both fully electric and hybrid tractors. While pure electric tractors are typically limited by battery capacity and suited for small to medium horsepower applications, hybrid electric configurations are better equipped to handle the demands of high-horsepower tractors used on large-scale farms [3-5]. Effective energy management plays a crucial role in this context, focusing on the optimal distribution of power among available sources based on specific power requirements [6]. This approach aims to achieve fuel savings and reduce consumption throughout the operational cycle. Unlike automobiles, which operate on structured roads, tractors function in varied and specialized agricultural environments, requiring customized energy management strategies to maximize performance across diverse field conditions [7, 8].

Tractors operate in two primary cycles: the working cycle in fields and the transport cycle on roads. The working cycle encompasses various phases, including seeding, ploughing, rototilling, harvesting, and other tasks, each characterized by varying load demands [9]. Research indicates that tractors spend over 80% of their operational lifespan within a specific speed range [10, 11]. In the context of non-plug-in

hybrid tractors, energy management is challenged by the limited capacity of the onboard electrical system, despite the tractor's consistently high-power demands, which often keep the engine in a starting state. Energy management strategies have been widely implemented based on controlling rules to address these challenges in hybrid tractor systems.

This study aims to reduce fuel consumption in Solid Oxide Fuel Cell-based Hybrid Electric Tractors (SOFC-HET) through a hybrid methodology that comprehensively optimizes input variables, promoting a more sustainable and resource-efficient operation. To validate the proposed approach, the system is tested using the MATLAB platform and benchmarked against other methods. During ploughing operations, with initial State of Charge (SOC) levels of 40%, 65%, and 90%, the hydrogen tank capacity under the proposed technique is indicated at 6.457 kg.

2. SYSTEM DYNAMIC MODELS

A. Tractor Model

Figure 1 depicts the longitudinal forces on the tractor during ploughing. The traction of the tractor F_t is formulated using Equations (1) and (2) [20].

$$F_t = F_f + F_i + F_j + F_{plg} \quad (1)$$

$$P_{req} = \frac{F_t V}{1000\eta_{mec}} + P_{sl} \quad (2)$$

where, rolling resistance is expressed as F_f, slope resistance is denoted as F_i, acceleration resistance is denoted as F_j, ploughing traction resistance is represented as F_{plg}, tractor power demand is denoted as P_{req}, tractor operating speed is specified as 'V', mechanical transmission efficiency is expressed as η_{mec}, slip loss power is denoted as P_{sl} [22].

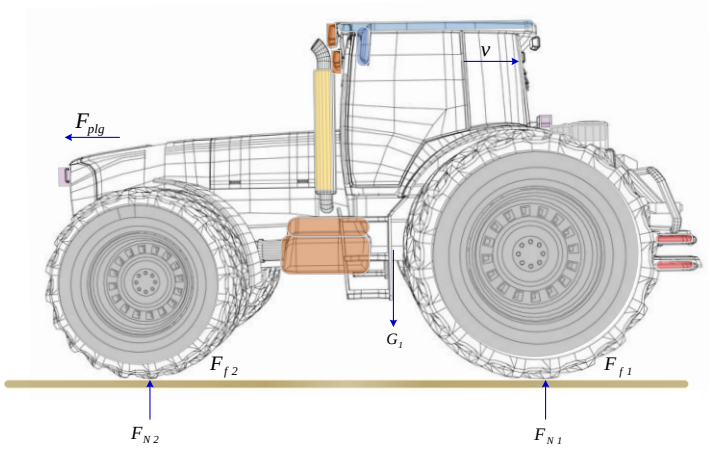

Figure 1: Longitudinal forces of the tractor during ploughing operation

In this study, a commonly employed empirical formula, represented by Equation (3) [23-25], is chosen to elucidate the ploughing resistance.

$$F_{plg} = z * b * h * k \quad (3)$$

where number of ploughshares is denoted as 'z', single ploughshare width is expressed as 'b', depth for ploughing is expressed as 'h', soil specific resistance is denoted as 'k'.

The power demand from drive cycle P_{cycle} is expressed in the Equation [28].

$$P_{cycle}(t) = v\left(F_a(t) + F_r(t) + F_g(t) + m_v(t)\frac{d}{dt}v(t)\right) \quad (4)$$

where F_r expresses rolling friction, F_a denotes aerodynamic friction, F_g denotes gravity force, vehicle speed is denoted as 'v', mass of the vehicle is represented as m_v, time is denoted as 't'.

$$F_a = 0.5v^2AC_x\rho \quad (5)$$

$$F_r = C_r m_v g\cos(\alpha) \quad (6)$$

$$F_g = m_v g\sin(\alpha) \quad (7)$$

where aerodynamic drag coefficient is expressed as C_r, drag coefficient is expressed as C_x, road slope is denoted as α, vehicle front surface is specified as 'A', 'g' defines gravitational acceleration, air density

is expressed as ρ. DC bus power demand P_{demand} must be satisfied by three power sources using the following equation.

$$P_{demand} = \frac{P_{cycle}}{\eta_{DC/AC} * \eta_{motor}} \quad (8)$$

where $\eta_{DC/AC}$ denotes converter efficiency, motor efficiency is expressed as η_{motor}.

Figure 2 illustrates the proposed controller for the Fuel Cell Hybrid Tractor (FCHT) architecture, featuring a battery and a DC/DC converter. The Solid Oxide Fuel Cell (SOFC) serves as the primary component, converting chemical energy from hydrogen and oxygen into electrical energy. It is linked to the DC bus through a unidirectional converter. A supercapacitor is connected to the DC bus through a bidirectional converter, enabling both charging and discharging operations. Additionally, the battery is connected to the DC bus, playing a crucial role in stabilizing and maintaining the DC bus voltage [26-27].

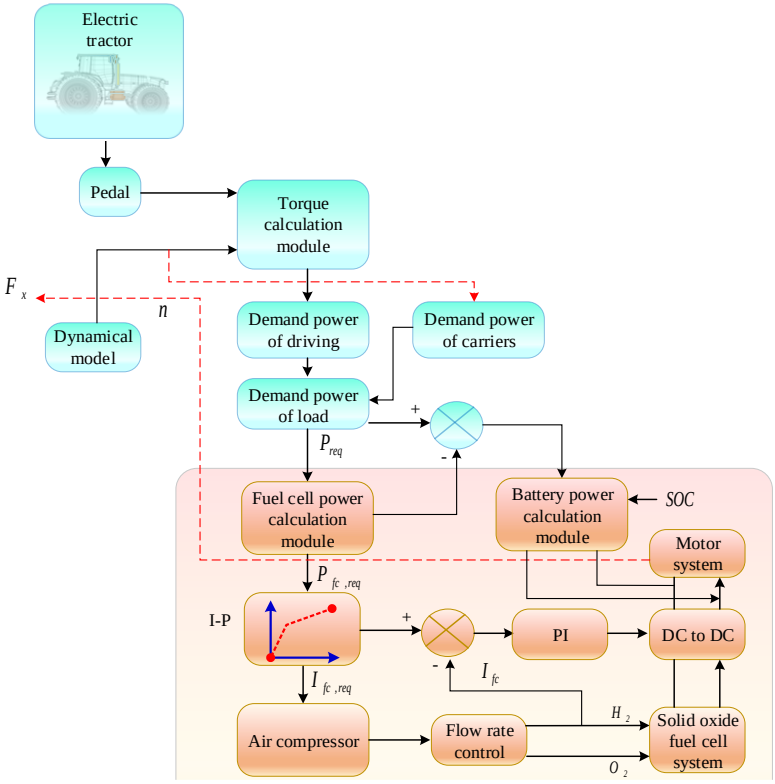

Figure 2: Proposed controller for FCHET architecture with battery and DC/DC converter

B. SOFC Model

Following Faraday law, SOFC hydrogen consumption $\dot{n}_{H_{2-c}}$, denoted as (mol/s), is computed as:

$$\dot{n}_{H_{2-c}} = \frac{iA}{n_e F} \quad (9)$$

If the fuel utilization factor is denoted as U_f, the supplied hydrogen is calculated as:

$$\dot{n}_{H_{2-s}} = \frac{\dot{n}_{H_{2-c}}}{U_f} = \frac{iA}{n_e F U_f} \quad (10)$$

The molar flow rate of the air stream is then determined as:

$$\dot{n}_{a-in}(O_2) = \dot{n}_{H_{2-s}} \frac{U_f/_2}{U_a} \quad (11)$$

The fuel stream molar flow rate is necessary to generate the supplied amount of hydrogen is then calculated as:

$$\dot{n}_{f-in} = \frac{\dot{n}_{H_{2-s}}}{x_{fc}} = \frac{iA}{n_e F U_f x_{fc}} \quad (12)$$

Therefore, the number of moles of hydrogen produced/fuel mole supplied to the system is expressed as follows:

$$x_{fc} = x_{H_2} + x_{CO} + 4x_{CH_4} \quad (13)$$

The cell voltage V_{cell} is derived as follows:

$$E_{nernst} - \Delta V_{act} - \Delta V_{ohm} - \Delta V_{conc} \leftarrow V_{cell} \quad (14)$$

where, open circuit voltage is represented as E_{nernst}, V_{act} denotes activated cell voltage, V_{ohm} denotes ohmic losses, V_{conc} represents concentrated cell voltage, current density is termed as i_{fc} [34-36].

$$E_{nernst} = E_o + \frac{RT}{F}\left(\frac{P_{H_2}P_{O_2}^{0.5}}{P_{H_2O}}\right) \quad (15)$$

where standard potential is expressed as E_o, 'R' denotes universal gas constant, operating temperature is expressed as 'T', 'F' denotes faraday constant, P_{H_2}, P_{O_2},P_{H_2O} expresses partial pressures.

The Current density is derived as:

$$i_{fc} = i_o\left(e^{(\alpha_1 F/RT)V_{act}} - e^{(\alpha_2 F/RT)V_{act}}\right) \quad (16)$$

$$V_{act} = \frac{RT}{n\alpha F}\ln\left({}^{i_{fc}}/_{2i_o} + \sqrt{(i_{fc}/2i_o)^2 + 1}\right) \quad (17)$$

Where $\alpha_1$is made equal to α_2 for implementation purpose, $i_O$denotes exchange current density, limiting current density of the SOFC is expressed as i_L.

$$V_{conc} = -\frac{RT}{nF}\ln\left(1 - \frac{i_{fc}}{i_L}\right) \quad (18)$$

$$V_{ohmic} = \left(\gamma \exp\left[\beta\left(\frac{1}{T_o} - \frac{1}{T}\right)\right]\right) i_{fc} = r i_{fc} \quad (19)$$

where constant coefficients of fuel cell are denoted as γ and β, operating temperature of fuel cell is denoted as 'T', internal resistance is specified as 'r'.

C. Battery Model

The battery voltage$E(t)$ is expressed as the equation (20),

$$E(t) = E_{U,p} - E_{U,n} - E_{S,p} - E_{S,n} - E_e - E_{O,n} - E_{O,p} \quad (20)$$

where, $E_{U,p}$ and $E_{U,n}$ denotes equilibrium potentials, $E_{O,n}$ and $E_{O,p}$ denotes surface over-potentials arising from charge transfer resistance, voltage drop resulting from solid-phase ohmic resistance is formulated as $E_{S,p}, E_{S,n}, E_e$. Equilibrium potential $E_{U,e}$ is calculated as the Nernst equation (21):

$$E_{U,e} = U_0 + \frac{RT_{elec}}{nF}\ln\left(\frac{1-x_e}{x_e}\right) + E_{act,e} \quad (21)$$

where, electrode is denoted as 'e' (negative for 'n', positive for 'p'), reference voltage is expressed as U_0, electrode temperature is specified as T_{elec}, number of electrons is specified as 'n', activity correction term is denoted as $E_{act,i}$ [37-38].

D. DC-DC Converter Model

SOFC is connected to a DC/DC boost converter and each converter incorporates 2 IGBT transistors controlled by PWM signals. These Pulse Width Modulation (PWM) signals are computed based on reference currents for the SOFC. Equation (22) depicts the relationship between input as well as output power.

$$i_o = \eta_{conv}\frac{P_{in}}{U_o} \quad (22)$$

where input power is denoted as P_{in}, output voltage is represented as U_o, DC to DC converter efficiency is denoted as η_{conv}, i_o represents output current.

E. Proposed Hybrid Approach for Fuel Consumption Minimization

In the research, a hybrid model is developed for minimizing the fuel consumption and to give the precise solution. The model combines a multi-head attention mechanism called IWaOT to effectively minimize energy consumption. Mathematically, the procedure is expressed as follows:

To tackle the challenge of inaccurate modelling, the optimal values for the control parameters are estimated by minimizing the SSE between the model's predicted fuel consumption and the empirically measured fuel consumption. The mathematical representation of this objective function is provided as [33]:

$$SSE = \sum_{m=1}^{N_{samples}}[\,n_{f,exp}(m) - \,n_{f,est}(m)]^2 \quad (23)$$

Table 1: Parameters bound

Parameters	Upper Bound	Lower Bound
Battery SoC, SOC (%)	90	20
Power Demand, P_Demand_TOTAL (kW)	21	4.5
FC Power, P_fc (kW)	22	13.6

F. Improved Walrus Optimization Technique (IWaOT)

This section presents the mathematical model underlying the Improved Walrus Optimization Technique (IWaOT). A set of randomly generated candidate solutions, X are initiated with the optimization process,

as described in Equation (24). This initial population forms the foundation for exploring the solution space and iteratively improving toward the optimal solution [33].

$$X = LL + \text{rand}(UL - LL) \quad (24)$$

Here, rand represents a uniform random vector with values ranging from 0 to 1, while LL and UL denote the lower and upper bounds of the problem parameters, respectively. The optimization process is carried out by agents referred to as walruses, whose positions are iteratively updated to explore and exploit the solution space. This iterative position adjustment enables the walruses to converge toward the optimal solution over successive iterations.

$$X = \begin{bmatrix} X_{1,1} & X_{1,2} & \dots & X_{1,d} \\ X_{2,1} & X_{2,2} & \cdots & X_{2,d} \\ \vdots & & \ddots & \vdots \\ \dots & & \dots & \dots \\ X_{n,1} & X_{n,2} & \cdots & X_{n,d} \end{bmatrix}_{nxd} \quad (25)$$

Here, d represents the dimension of the design variables, and n denotes the population size. The fitness values corresponding to all search agents are evaluated to assess the quality of each candidate solution. The fitness evaluation is performed using the following expression:

$$F = \begin{bmatrix} f_{1,1} & f_{1,2} & \dots & f_{1,d} \\ f_{2,1} & f_{2,2} & \cdots & f_{2,d} \\ \vdots & & \ddots & \vdots \\ \dots & & \dots & \dots \\ f_{n,1} & f_{n,2} & \cdots & f_{n,d} \end{bmatrix}_{nxd} \quad (26)$$

The population of Walrus consists of 90% adults and 10% juveniles. Among the adult population, the male-to-female ratio is evenly balanced at 1:1. Walruses are extremely vigilant. During patrolling by Walruses and in case any unforeseen circumstances are discovered, warning signals are launched. The danger and safety signals in Walrus optimization are defined as follows:

Danger Signal = A * R

$$\alpha = 1 - t/T \quad (27)$$

$$A = 2 * \alpha \quad (28)$$

$$R = 2 * r_1 - 1 \quad (29)$$

Here, T is the maximum number of iterations, *A* and *R* are danger factors, α is defined from 1 to 0 and t denotes the number of iterations.

The Safety signal in Walrus optimization that corresponds to the danger signal is defined as:

Safety Signal = r_2

where r_2 and r_1 are random values and fall in the interval (0,1).

When danger factors become too high, a group of Walruses move to locations which are better suited for population survival. The Walrus position during this phase is updated as follows:

$$X_{i,j}^{t+1} = X_{i,j}^{t} + \text{Migration step} \quad (30)$$

$$\text{Migration step} = (X_m^t - X_n^t) . \beta . r_3^2 \quad (31)$$

$$\beta = 1 - \frac{1}{1+\exp\left(\frac{t-\frac{T}{2}}{\frac{T}{10}}\right)} \quad (32)$$

Here, the current location of the *i*th walrus in the *j*th dimension is represented by $X_{i,j}^t$, and the new position is represented by $X_{i,j}^{t+1}$. The migration step refers to the step size of a walrus's movement during the optimization process. To guide this movement, two vigilantes—representative walruses—are randomly selected from the population. Their positions match X_m^t and X_n^t. β is the migration step control factor, which varies iteratively as a smooth curve. r_3 is a random number that falls between 0 and 1.

When danger levels are low, walrus herds generally prefer to reproduce within ocean currents rather than migrate. This behaviour allows them to conserve energy and focus on reproduction while remaining in safer, resource-rich environments. The lead Walrus (X_{best}^t) and the male Walrus ($Male_{i,j}^t$) have an influence on the female Walrus during reproduction, according to the position update of female walruses. The female walrus becomes increasingly influenced by the leader and less by her mate during the course os action.

$$Female_{i,j}^{t+1} = Female_{i,j}^{t} + \alpha . \left(Male_{i,j}^{t} - Female_{i,j}^{t}\right) + (1 - \alpha) . \left(X_{best}^{t} - Female_{i,j}^{t}\right) \quad (33)$$

where $\mathrm{Male}_{i,j}^{t}$ and $\mathrm{Female}_{i,j}^{t}$ are the positions of the *i*th male and female walruses in the *j*th dimension, and $\mathrm{Female}_{i,j}^{t+1}$ is the new position for the *i*th female walrus in the *j*th dimension. Juvenile

Walruses are targeted by Killer whales and polar bears near the edges of the herd. To avoid these predators, juvenile walruses must adapt by repositioning themselves within the group, seeking safety closer to the centre of the population.

$$\mathrm{Juvenile}_{i,j}^{t+1} = \left(O - \mathrm{Juvenile}_{i,j}^{t}\right) . P \quad (34)$$

Here P is the juvenile walrus's distress coefficient, and is a random number between 0 and 1, O is the reference safety position, LF is a vector of random values that represent Lévy movement based on a Lévy distribution, and $\mathrm{Juvenile}_{i,j}^{t+1}$ is the new position for the *i*th juvenile walrus in the *j*th dimension.

$$\mathrm{Levy(a)} = 0.05 \times \frac{x}{|y|^{\frac{1}{a}}} \quad (35)$$

where y and x are two normally distributed parameters, x N(0,$\sigma x2$),y N(0, $\sigma y2$).

$$\sigma_x = \left[\frac{\Gamma(1+\alpha)\sin\left(\frac{\pi\alpha}{2}\right)}{\Gamma\left(\frac{1+\alpha}{2}\right)\alpha 2^{\frac{\alpha-1}{2}}}\right]^{\frac{1}{\alpha}}, \ \sigma_y = 1; \ \alpha = 1.5 \quad (36)$$

where σ_x and σ_y are the standard deviations, $\Gamma(x) = (x+1)!$.

Natural predators often target walruses during their underwater feeding activities. In response to danger warnings from their peers, walruses will abandon their current feeding area. This defensive behaviour is reflected in the later iterations of the Improved Walrus Optimization Technique (IWaOT), where a controlled level of population disturbance enhances the algorithm's exploratory capabilities, mirroring the walruses' adaptive behaviour in their natural environment. Here, the distance between the best and current walrus is shown by $|X_{best}^{t} - X_{i,j}^{t}|$, and r_4 is a random value that falls between 0 and 1.

In addition to their defensive strategies, walruses exhibit social gathering behaviour by cooperating during foraging and migration. By sharing location information, they help the entire herd identify regions of the sea with abundant food sources. This collaborative approach enhances the group's efficiency in resource acquisition, a trait that inspires the cooperative mechanisms within the Improved Walrus Optimization Technique (IWaOT).

$$X_{i,j}^{t+1} = (X_1 + X_2)/2 \quad (37)$$

$$X_1 = X_{best}^{t} - a_1 \times b_1 \times \left|X_{best}^{t} - X_{i,j}^{t}\right| \quad (38)$$

$$X_2 = X_{second}^{t} - a_2 \times b_2 \times \left|X_{second}^{t} - X_{i,j}^{t}\right| \quad (39)$$

$$a = \beta \times r_5 - \beta \quad (40)$$

$$b = \tan(\theta) \quad (41)$$

where X_{second}^{t} represents the position of the second Walrus in the current iteration, $|X_{second}^{t} - X_{i,j}^{t}|$ equals the distance between the current walrus and the second walrus, a and b are the gathering coefficients, and X_1 and X_2 are two weights influencing the walrus's gathering behaviour. The random number r_5 varies between 0 and 1, while the values of θ span from 0 to π.

The flowchart of IWaOT is described in detail in Figure 3.

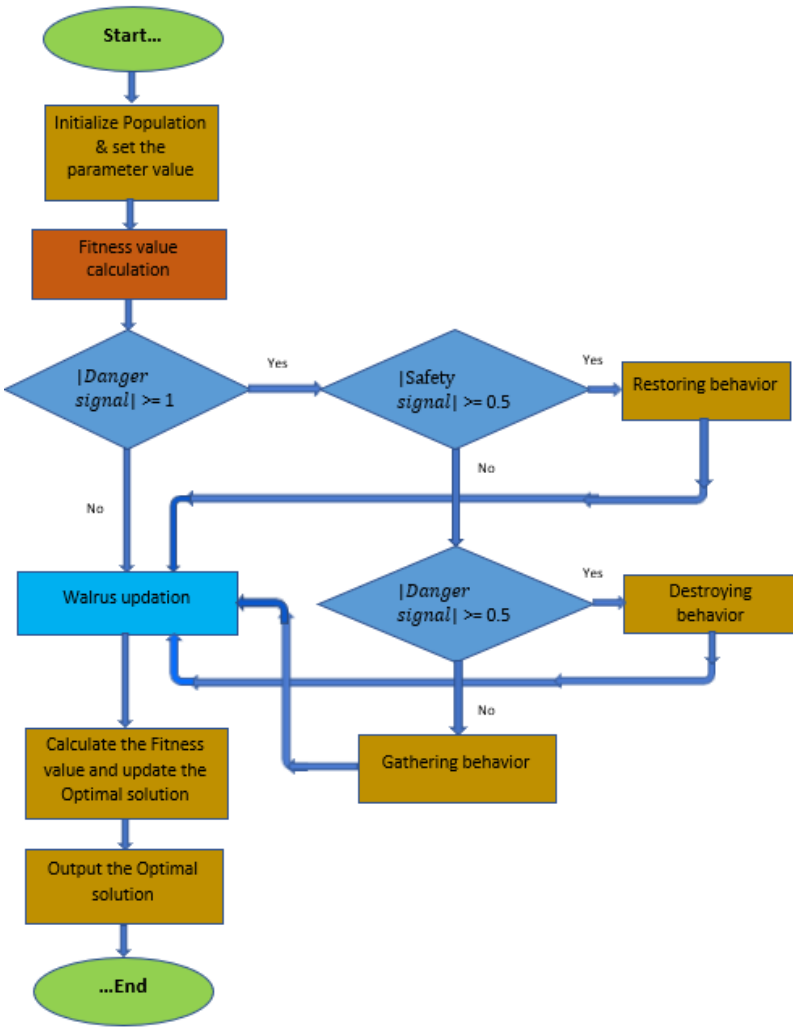

Figure 3: Architecture of IWaOT

3. RESULTS AND DISCUSSION

The proposed IWaOT technique's performance is executed in the MATLAB platform and benchmarked against other methodologies. The performance analysis is carried out based on plough results at 200 sec before and after optimization. The parameters like SOFC power, motor power, hydrogen consumption, battery output power, battery SOC, SOFC stack efficiency, total and net power demand, battery voltage and current are analysed in the study. Table 2 illustrates the parameters used in the implementation. The graphical representation is explained in the following:

Table 2: Implementation parameters

Parameters	Values	Units
Nominal value for SOFC	13625	W
Maximal value for SOFC	53040	W
SOFC resistance	0.097297	ohms
Nerst voltage of one cell	1.0989	V
Fuel	137.6	slpm
Air	327.5	slpm
Exchange current	0.7173	A
Exchange coefficient	0.32573	-
Nominal fuel flow rate	118.8	lpm
Maximum fuel flow rate	592.8	lpm
Nominal air flow rate	885	lpm
Maximum air flow rate	4418	lpm
Fuel supply pressure	1.5	bar
Air supply pressure	1	bar
Operating temperature	800	Celsius

Plough Results at 200sec: After Optimization

The ploughing total and net power demand of the tractor fluctuates wildly between 20 to 200 seconds. The total power demand at SOC=65% using proposed approach achieves the higher value of 2×10^4W. The net power demand at SOC=65% using proposed approach achieves the higher value of 17500W.

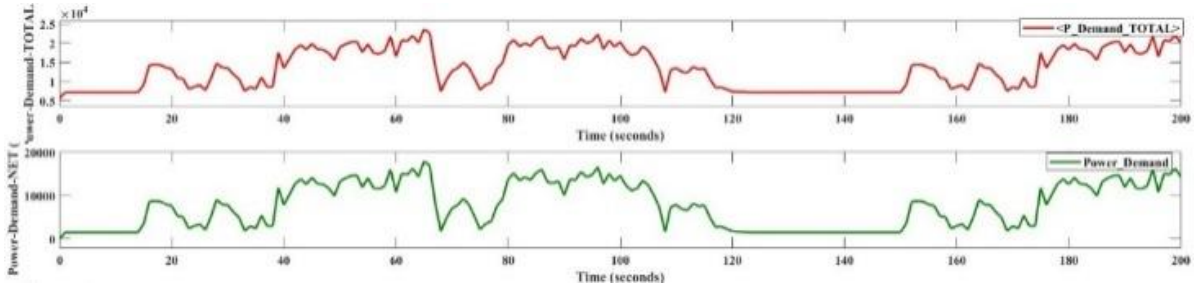

Figure 4: Total and net power demand at SOC=65% using proposed approach

SOFC power variation versus time at SOC=65% using proposed approach is shown in Figure 5. The SOFC begins with a higher power output, approximately 2.3×10^{-4} W compared to the 1.4×10^4 W before optimization. It peaks at around 2.3×10^4 W between 40 and 60 seconds, a notable increase by using the proposed technique. The power output maintains a relatively stable range between 1.4×10^4 W and 2.3×10^4 for 200 seconds. Similarly, hydrogen consumption maintains a range between 1.8×10^{-4} kg/sec and 2.97×10^{-4} kg/sec for 200 seconds.

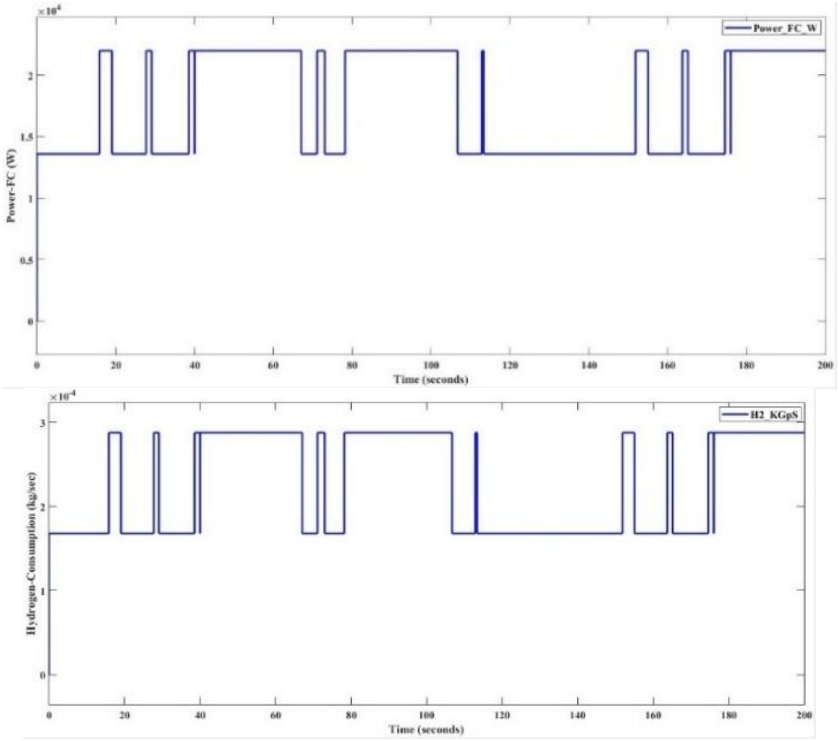

Figure 5: SOFC power variation and Hydrogen consumption variation versus time at SOC=65% using proposed approach

Battery output power variation at SOC=65% using proposed approach is shown in Figure 6. Battery starts at a power consumption of approximately 3600 W when SOC is 65%. The power consumption fluctuates more as compared to before optimization, maintaining power consumption between 0 W and 3600 W.

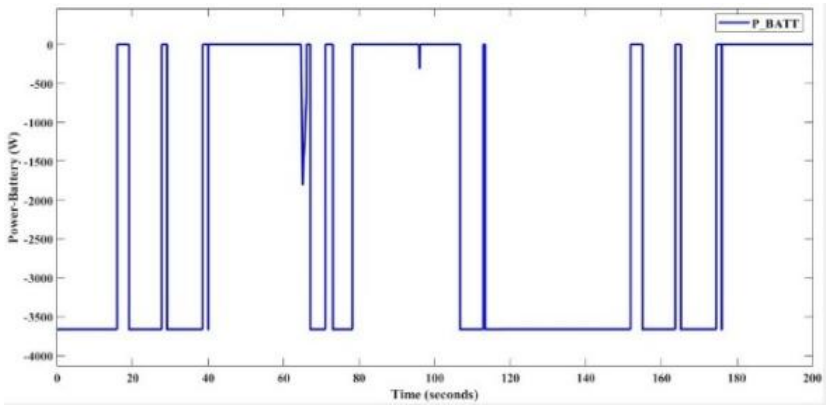

Figure 6: Battery output power variation at SOC=65% using proposed approach

Battery SOC power variation at SOC=65% using proposed approach is shown in Figure 7. The battery starts at an SOC of 65%. The SOC starts to increase at the time instant of 20 seconds due to regeneration and after that the battery SOC gradually decreases to 64% level.

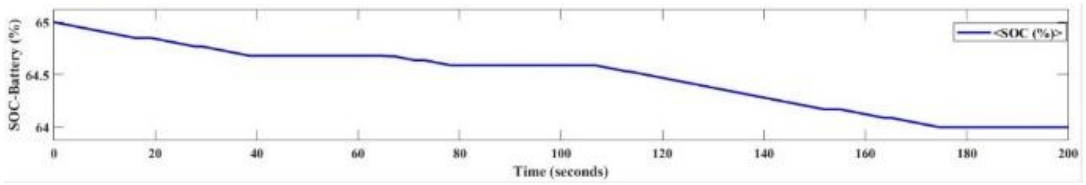

Figure 7: Battery SOC power variation at SOC=65% using proposed approach

SOFC stack efficiency variation at SOC=65% using proposed approach is shown in Figure 8. Initiating at an efficiency of approximately 67.5%, similar to the pre-optimization state, the SOFC stack exhibits cyclic variation in efficiency. By the end of 200 seconds, the stack efficiency is approximately 64.8%, a significant improvement compared to the 40% efficiency observed before optimization.

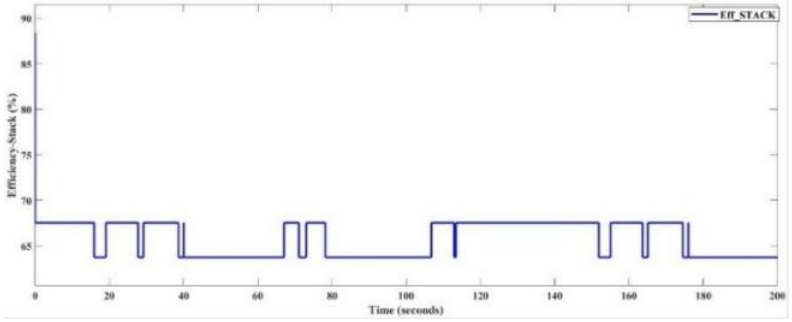

Figure 8: SOFC stack efficiency variation at SOC=65% using proposed approach

Table 3: Comparison of various solution techniques in terms of SOC

Initial SOC	Final SOC			
	Before optimization	ECMS [43]	FA-ECMS [43]	IWaOT
40%	44.2%	-	-	42%
60%	-	60.75%	60.27%	-
65%	65.84%	-	-	65.4%
90%	90%	-	-	90%

The hydrogen tank capacity during ploughing using proposed technique is estimated 6.457kg against 9.596kg before optimization. Comparison of various solution techniques in terms of SOC is shown in Table 3. During ploughing cycle, the battery SOC is 60.75% when employing the traditional ECMS (Equivalent Consumption Minimization Strategy) and slightly lower at 60.27% with the FA-ECMS (Fuzzy Adaptive-ECMS). Using proposed IWaOT approach, battery SOC for target levels of 40%, 65%, and 90% is determined to be 42%, 65.4%, and 90%, respectively, ensuring effective power maintenance. The advantage with IWaOT lies in usage of optimized Hydrogen consumption with better performance.

Notably, the proposed strategy demonstrates the battery power closely tracking the target SOC after the working cycle, showcasing superior performance.

4. CONCLUSION

The research endeavours to enhance the efficiency and reduce fuel consumption in SOFC-HET through a comprehensive hybrid approach. IWaOT plays a pivotal role in forecasting the tractor power demand and fuel cell operating conditions, enabling optimized control of power distribution, fuel flow, air flow, and temperature. The integration of SHO directly targets the optimization of control parameters, effectively minimizing fuel consumption and addressing hydrogen fuel consumption concerns. The proposed approach demonstrates increased efficiency and an extended lifespan for the FC system. Implementation in the MATLAB platform and comparison with other approaches validate the feasibility of IWaOT. Furthermore, the research findings reveal specific hydrogen tank capacities during ploughing under varying initial SOC levels. According to the proposed strategy, the SOC value targets at 60% at all levels and achieves an equilibrium at all states of battery SOC. The proposed strategy contributes to achieving greater SOFC efficiency of 67.5% after optimization against 62.5% before optimization and an extended lifespan for the SOFC system after optimization when compared with before optimization. In future endeavours, the research will undertake experiments considering influence of temperature on battery and hydraulic component efficiency and validates the reliability analysis in real-world application environments.

References

[1]Xu, L., Huangfu, Y., Ma, R., Xie, R., Song, Z., Zhao, D., Yang, Y., Wang, Y. and Xu, L., 2022. A Comprehensive Review on Fuel Cell UAV Key Technologies: Propulsion System, Management Strategy and Design Procedure. IEEE Transactions on Transportation Electrification.

[2] Zhou, Q., Li, J., Shuai, B., Williams, H., He, Y., Li, Z., Xu, H. and Yan, F., 2019. Multi-step reinforcement learning for model-free predictive energy management of an electrified off-highway vehicle. Applied Energy, 255, p.113755.

[3] Zhou, Y., Ravey, A. and Péra, M.C., 2021. Real-time cost-minimization power-allocating strategy via model predictive control for fuel cell hybrid electric vehicles. Energy Conversion and Management, 229, p.113721.

[4] Du, C., Huang, S., Jiang, Y., Wu, D. and Li, Y., 2022. Optimization of energy management strategy for fuel cell hybrid electric vehicles based on dynamic programming. Energies, 15(12), p.4325.

[5] Tian, X., Cai, Y., Sun, X., Zhu, Z. and Xu, Y., 2019. An adaptive ECMS with driving style recognition for energy optimization of parallel hybrid electric buses. Energy, 189, p.116151.

[6] Rodriguez, R., Trovao, J.P.F. and Solano, J., 2022. Fuzzy logic-model predictive control energy management strategy for a dual-mode locomotive. Energy Conversion and Management, 253, p.115111.

[7] Yang, Y., Xu, Y., Zhang, H., Yang, F., Ren, J., Wang, X., Jin, P. and Huang, D., 2022. Research on the energy management strategy of extended range electric vehicles based on a hybrid energy storage system. Energy Reports, 8, pp.6602-6623.

[8] Xie, B., Wang, S., Wu, X., Wen, C., Zhang, S. and Zhao, X., 2022. Design and hardware-in-the-loop test of a coupled drive system for electric tractor. Biosystems Engineering, 216, pp.165-185.

[9] Xie, P., Tan, S., Guerrero, J.M. and Vasquez, J.C., 2021. MPC-informed ECMS based real-time power management strategy for hybrid electric ship. Energy Reports, 7, pp.126-133.

[10] Song, Y., Han, K. and Li, X., 2021. Study on the fuel economy of fuel cell electric vehicle based on rule-based energy management strategies. International Journal of Powertrains, 10(3), pp.266-292.

[11] Nassar, M.Y., Shaltout, M.L. and Hegazi, H.A., 2023. Multi-objective optimum energy management strategies for parallel hybrid electric vehicles: A comparative study. Energy Conversion and Management, 277, p.116683.

[12] Liu, Y., Liu, J., Qin, D., Li, G., Chen, Z. and Zhang, Y., 2020. Online energy management strategy of fuel cell hybrid electric vehicles based on rule learning. Journal of Cleaner Production, 260, p.121017.

[13] Wen, C.K., Zhang, S.L., Xie, B., Song, Z.H., Li, T.H., Jia, F. and Han, J.G., 2022. Design and verification innovative approach of dual-motor power coupling drive systems for electric tractors. Energy, 247, p.123538.

[14] Curiel-Olivares, G., Johnson, S.C., Escobar, G.E.R.A.R.D.O. and Schacht-Rodríguez, R.I.C.A.R.D.O., 2023. Model Predictive Control based Energy Management System for a Hybrid Electric Agricultural Tractor. IEEE Access.

[15] Zhang, S.L., Wen, C.K., Ren, W., Luo, Z.H., Xie, B., Zhu, Z.X. and Chen, Z.J., 2023. A joint control method considering travel speed and slip for reducing energy consumption of rear wheel independent drive electric tractor in ploughing. Energy, 263, p.126008.

[16] Radrizzani, S., Panzani, G., Trezza, L., Pizzocaro, S. and Savaresi, S.M., 2023. An Add-On Model Predictive Control Strategy for the Energy Management of Hybrid Electric Tractors. IEEE Transactions on Vehicular Technology.

[17] Zhang, C., Zhou, Q., Hua, M., Xu, H., Bassett, M. and Zhang, F., 2023. Cuboid equivalent consumption minimization strategy for energy management of multi-mode plug-in hybrid vehicles considering diverse time scale objectives. Applied Energy, 351, p.121901.
[18] Min, D., Song, Z., Chen, H., Wang, T. and Zhang, T., 2022. Genetic algorithm optimized neural network based fuel cell hybrid electric vehicle energy management strategy under start-stop condition. Applied Energy, 306, p.118036.
[19] da Silva, S.F., Eckert, J.J., Silva, F.L., Silva, L.C. and Dedini, F.G., 2021. Multi-objective optimization design and control of plug-in hybrid electric vehicle powertrain for minimization of energy consumption, exhaust emissions and battery degradation. Energy Conversion and Management, 234, p.113909.
[20] Ajay Ahuja, D. R. Waghole and Sushil S. Ramdasi, "Optimal Control Strategy for PEM Hybrid Electric Vehicle using Matlab Simulink", Journal of Electrical Electronics Engineering, April 2023.
[21] Ajay Ahuja, D.R. Waghole and Sushil S. Ramdasi, "Fuel Cell Technologies for Automotive Applications", STM Journal of Power Electronics & Power Systems, 2022.
[22] Chen, Y., Xie, B., Du, Y. and Mao, E., 2019. Powertrain parameter matching and optimal design of dual-motor driven electric tractor. International Journal of Agricultural and Biological Engineering, 12(1), pp.33-41.
[23] Geng, C., Jin, X. and Zhang, X., 2019. Simulation research on a novel control strategy for fuel cell extended-range vehicles. International Journal of Hydrogen Energy, 44(1), pp.408-420.
[24] Farhadi Gharibeh, H. and Farrokhifar, M., 2021. Online multi-level energy management strategy based on rule-based and optimization-based approaches for fuel cell hybrid electric vehicles. Applied Sciences, 11(9), p.3849.
[25] Liu, J., Chen, Y., Li, W., Shang, F. and Zhan, J., 2017. Hybrid-trip-model-based energy management of a PHEV with computation-optimized dynamic programming. IEEE Transactions on Vehicular Technology, 67(1), pp.338-353.
[26] Wang, Y., Advani, S.G. and Prasad, A.K., 2020. A comparison of rule-based and model predictive controller-based power management strategies for fuel cell/battery hybrid vehicles considering degradation. International Journal of Hydrogen Energy, 45(58), pp.33948-33956.
[27] Mocera, F., 2020. A model-based design approach for a parallel hybrid electric tractor energy management strategy using hardware in the loop technique. Vehicles, 3(1), pp.1-19.
[28] Feng, Y. and Dong, Z., 2020. Optimal energy management with balanced fuel economy and battery life for large hybrid electric mining truck. Journal of Power Sources, 454, p.227948.
[29] Mocera, F. and Somà, A., 2020. Analysis of a parallel hybrid electric tractor for agricultural applications. Energies, 13(12), p.3055.
[30] Yang, H., Sun, Y., Xia, C. and Zhang, H., 2022. Research on Energy Management Strategy of Fuel Cell Electric Tractor Based on Multi-Algorithm Fusion and Optimization. Energies, 15(17), p.6389.
[31] Anbarasu, A., Dinh, T.Q. and Sengupta, S., 2022. Novel enhancement of energy management in fuel cell hybrid electric vehicle by an advanced dynamic model predictive control. Energy Conversion and Management, 267, p.115883.
[32] Liang, Y., Liang, Q., Zhao, J. and He, J., 2022. Minimum hydrogen consumption power allocation strategy for the multi-stack fuel cell (MFC) system based on a discrete approach. Frontiers in Energy Research, 10, p.966852.
[33] Essam H. Houssein, Nagwan Abdel Samee, Maali Alabdulhafith and Mokhtar Said, Extraction of PEM fuel cell parameters using Walrus Optimizer, AIMS Mathematics, DOI: 10.3934/math.2024622, April 2024.
[34] Yu, P., Li, M., Wang, Y. and Chen, Z., 2022. Fuel cell hybrid electric vehicles: A review of topologies and energy management strategies. World Electric Vehicle Journal, 13(9), p.172.
[35] Li, C., Hu, G., Zhu, Z., Wang, X. and Jiang, W., 2022. Adaptive equivalent consumption minimization strategy and its fast implementation of energy management for fuel cell electric vehicles. International Journal of Energy Research, 46(11), pp.16005-16018.
[36] Alcázar-García, D. and Martínez, J.L.R., 2022. Model-based design validation and optimization of drive systems in electric, hybrid, plug-in hybrid and fuel cell vehicles. Energy, 254, p.123719.
[37] Beligoj, M., Scolaro, E., Alberti, L., Renzi, M. and Mattetti, M., 2022. Feasibility evaluation of hybrid electric agricultural tractors based on life cycle cost analysis. IEEE Access, 10, pp.28853-28867.
[38] Mocera, F. and Somà, A., 2020. Analysis of a parallel hybrid electric tractor for agricultural applications. Energies, 13(12), p.3055.
[39] Medževeprytė, U.K., Makaras, R. and Rimkus, A., 2022. Efficiency of an off-road heavy-duty series hybrid drive based on a modified world harmonized transient cycle. Transport problems, 17(4), pp.187-195.
[40] Zhang, J., Feng, G., Xu, L., Yan, X., Wang, W. and Liu, M., 2023. Energy-saving control of hybrid tractors based on instantaneous optimization. World Electric Vehicle Journal, 14(2), p.27.
[41] Zhang, J., Feng, G., Liu, M., Yan, X., Xu, L. and Shang, C., 2023. Research on Global Optimal Energy Management Strategy of Agricultural Hybrid Tractor Equipped with CVT. World Electric Vehicle Journal, 14(5), p.127.
[42] Xu, W., Liu, M., Xu, L. and Zhang, S., 2022. Energy Management Strategy of Hydrogen Fuel Cell/Battery/Ultracapacitor Hybrid Tractor Based on Efficiency Optimization. Applied Sciences, 13(1), p.151.
[43] Zhu, Z., Zeng, L., Chen, L., Zou, R. and Cai, Y., 2022. Fuzzy Adaptive Energy Management Strategy for a Hybrid Agricultural Tractor Equipped with HMCVT. Agriculture, 12(12), p.1986.